JCTC Journal of Chemical Theory and Computation

ACS AUTHORCHOICE

pubs.acs.org/JCTC Article

Kinetic Isotope Effect in Low-Energy Collisions between Hydrogen Isotopologues and Metastable Helium Atoms: Theoretical Calculations Including the Vibrational Excitation of the Molecule

Mariusz Pawlak,* Piotr S. Żuchowski, and Piotr Jankowski

Cite This: *J. Chem. Theory Comput.* 2021, 17, 1008−1016 Read Online

ACCESS | Metrics & More | Article Recommendations | Supporting Information

ABSTRACT: We present very accurate theoretical results of Penning ionization rate coefficients of the excited metastable helium atoms (^{4}He(2^3S) and ^{3}He(2^3S)) colliding with the hydrogen isotopologues (H_2, HD, D_2) in the ground and first excited rotational and vibrational states at subkelvin regime. The calculations are performed using the current best *ab initio* interaction energy surface, which takes into account the nonrigidity effects of the molecule. The results confirm a recently observed substantial quantum kinetic isotope effect (*Nat. Chem.* 2014, 6, 332−335) and reveal that the change of the rotational or vibrational state of the molecule can strongly enhance or suppress the reaction. Moreover, we demonstrate the mechanism of the appearance and disappearance of resonances in Penning ionization. The additional model computations, with the morphed interaction energy surface and mass, give better insight into the behavior of the resonances and thereby the reaction dynamics under study. Our theoretical findings are compared with all available measurements, and comprehensive data for prospective experiments are provided.

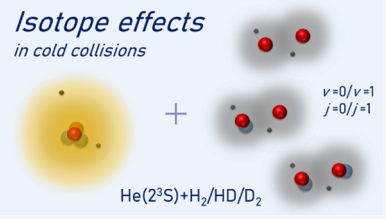

1. INTRODUCTION

A chemical reaction is a fundamental process in chemistry. External control of its dynamics is crucial to understand many physical and chemical phenomena, especially at the quantum level. Recent sophisticated merged beams experiments for low-energy atom−molecule collisions revealed the possibility of controlling molecular reactions.[1−10] These experiments were groundbreaking achievements in cold chemistry.[11−15] The first merged neutral supersonic beams technique was demonstrated in 2012 by the group of Narevicius,[1] approaching a collision temperature below 10 mK. Narevicius and co-workers investigated the Penning ionization (PI) reactions by colliding excited metastable helium atoms ^{4}He* (≡ ^{4}He(2^3S)), contained in one beam, with ground-state molecular hydrogen H_2, contained in another beam

$$He^* + H_2 \rightarrow He + H_2^+ + e^-$$

They observed a few shape resonances by measuring reaction rate coefficients, systematically decreasing collision energy from a few tens of kelvins down to millikelvins. In follow-up studies, they focused on the isotope effect,[2] where the hydrogen molecule was substituted by hydrogen deuteride (HD) and deuterium (D_2). This was the first observation of such an effect in low-energy collisions. It turned out that the positions of the resonances were different for the hydrogen isotopologues, far from intuitive expectations. The substitution strongly affected the PI process with an order of magnitude increase in the reaction rate coefficient at certain collision energies. This effect may significantly matter to the isotopic composition and formation of interstellar clouds and structure.[16,17]

Hydrogen and helium are the lightest and most abundant chemical elements in the Universe, while molecular hydrogen is the lightest and the most common molecule.[18,19] For instance, molecular hydrogen and helium are the prime constituents of gas giants.[20] New ground- and space-based high-resolution telescopes enable the observation of light elements, which was previously inaccessible. Very recently, scientists have made the first-ever detection of 2^3S helium in the atmosphere of one of the planets (WASP-107b) beyond the solar system.[19] Soon after, excited metastable helium was confirmed on other exoplanets.[21−29] The measurements of the helium absorption signal in exoplanet atmospheres are now important markers of a variety of planetary processes. They have become a unique probe for assessing exoplanetary compositions and understanding the formation of exoplanetary systems. The observation of long-lived metastable helium atoms has changed the way astronomers look at exoplanets and has raised the significance of theoretical chemistry for astrophysical domains. Undoubtedly, the collisions of 2^3S helium with various atomic and molecular partners, especially with hydrogen isotopologues, are of primary importance for

Received: October 26, 2020
Published: January 21, 2021

astrochemistry. It is also worth noting that there are a considerable number of experimental studies for He* in collisions with more complex molecules (for example, hydrogen sulfide,[30] nitrous oxide,[31] benzene,[32] naphthalene,[33] anthracene,[33] [2,2]-paracyclophane,[34] pyrene,[35] chrysene,[35] coronene,[35] glycine,[36] anisole,[37] thioanisole,[37] and selenoanisole[37]).

As was shown in ref 2, the kinetic isotope effect in the collisions between light subsystems (such as ^{4}He* with H_2, HD, and D_2) is dramatic, fundamentally changing the reactivity of the PI process. A high level of theory is required to evaluate the experimental findings. The main motivation of our present studies was to confirm the strong isotope effect in cold chemistry reactions based on our recently developed, very accurate interaction energy surface.[38] This *ab initio* surface includes nonrigidity effects of the molecule, which play an important role in low-energy molecular anisotropic collisions.[38] Additionally, this surface also allows us to predict resonance structures for experimentally uncharted cases. Since we can account for nonrigidity effects, complexes with the vibrationally excited hydrogen molecule or its isotopologues can be considered. Such complexes have become easier to access experimentally due to recent progress in the production and the control of the excited hydrogen isotopologues.[39−41] Thus, in the present work, we compute reaction rate coefficients of the H_2/HD/D_2 molecules in the ground and excited rotational (j = 0/1) and vibrational (v = 0/1) states with ^{4}He*, and additionally with ^{3}He*. We demonstrate that by changing the quantum state of the molecule, one can turn on or off particular low-energy resonances, thereby strongly modify the PI. It enables us better control over reactions in the subkelvin regime.

2. THEORY

2.1. Interaction Energy Surface. Our theoretical approach consists of two parts: the first is to prepare the best possible interaction energy surface, and the second is to perform quantum-dynamical calculations of the PI rate coefficients. To parameterize the He* + H_2 complex, we use Jacobi coordinates: the distance R between He* and center of mass (COM) of H_2, the angle θ between the H_2 bond and the COM−He* direction, and the distance r between the hydrogen nuclei. Thus, the full-dimensional energy surface can be written as a function of these coordinates, $V(R, \theta, r)$. In our previous paper,[38] we have shown for ^{4}He* + H_2 that if the widely used rigid-rotor approximation is applied, one cannot achieve a quantitative agreement with experiment, even if state-of-the-art *ab initio* methods are employed to calculate the interaction energy surface. The rigid-rotor approximation procedure involves two stages: the construction of the interaction energy surface for rigid molecules, and scattering calculations limited to only intermolecular coordinates. We have demonstrated[38] that if the interaction energy surface averaged over the vibrations of the hydrogen molecule is used instead of the rigid-molecule surface, an excellent agreement with the experiment can be obtained, despite the rigid-rotor approximation in the scattering calculations. This is because though the vibrationally averaged surface depends only on the intermolecular coordinates, to calculate it one needs to know the dependence of the interaction energy also on the intramolecular coordinates. Thus, the surface includes effective information of the nonrigidity effects and is not equivalent to the rigid-monomer one. In principle, to calculate the vibrationally averaged surface, one needs to know a full-dimensional surface for a given complex,[42] however, the surface averaged over the vibrational state v can be obtained approximated[43] using a Taylor expansion of the interaction potential $V(R, \theta, r)$ with respect to the intramonomer coordinate r, around some reference value r_c

$$\langle V\rangle_{j,v}(R,\theta) \approx f_0(R,\theta) + f_1(R,\theta)(\langle r\rangle_{j,v} - r_c) + \frac{1}{2}f_2(R,\theta)(\langle r^2\rangle_{j,v} - 2\langle r\rangle_{j,v}r_c + r_c^2) \quad (1)$$

where $f_0(R, \theta) = V(R, \theta, r_c)$, $f_1(R, \theta) = \partial V(R, \theta, r)/\partial r$ at $r = r_c$, and $f_2(R, \theta) = \partial^2 V(R, \theta, r)/\partial r^2$ at $r = r_c$. The $\langle r\rangle_{j,v}$ and $\langle r^2\rangle_{j,v}$ symbols denote the averaged values of r and r^2 for the rovibrational states of H_2 defined by the quantum numbers j and v. In our investigations, we took r_c equal to the H−H distance averaged over the rovibrational ground state, i.e., $r_c = \langle r\rangle_{0,0}$ = 1.4487 Bohr. The values of f_1 and f_2 can be calculated on the grid of the intermolecular coordinates with the finite-difference method. The vibrationally averaged surfaces obtained within this approximation were used in bound-state calculations for the H_2−CO,[44−46] Ar−HF,[47] and N_2−HF[48] complexes, and an excellent, or at least, very good agreement of the theoretical spectra with experimental ones was observed. For the H_2−CO complex, scattering calculations were also performed[49] with the surface defined through eq 1, and an excellent agreement with the experimental data[50,51] and the full-dimensional results was achieved.

In the present study, we have used the values of the f_i expansion functions, where i = 0, 1, 2, calculated in ref 38. The details can be found in that paper, but here we would like to mention that the leading f_0 term was obtained using the coupled cluster method with singles, doubles, and perturbative triples (CCSD(T)), and improved with a full configuration interaction (FCI) correction. The f_1 and f_2 derivatives were calculated with the symmetry-adapted perturbation theory (SAPT) method.[53] As was demonstrated for the ^{4}He* + H_2 complex, the diagonal Born−Oppenheimer (DBO) correction[54] is significantly smaller than other contributions to f_0, so we neglected this correction in that work. Moreover, for the ^{4}He* + HD and ^{4}He* + D_2 complexes, the DBO correction can be expected to be even smaller than for ^{4}He* + H_2 due to the larger masses of HD and D_2 in comparison to H_2. Thus, we can still neglect the DBO correction, and the f_i functions therefore do not depend on masses of helium or hydrogen isotopologues.

According to eq 1, to obtain the vibrationally averaged surface $\langle V\rangle_{j,v}(R, \theta)$, we need to know the values of $\langle r\rangle_{j,v}$ and $\langle r^2\rangle_{j,v}$ for H_2, HD, and D_2, for the required vibrational states v of these molecules. Moreover, for the *ortho*-H_2 and *para*-D_2 cases, when the molecules are in the j = 1 rotational state, the averaging was done with the (j = 1, v) rovibrational wave functions of H_2 and D_2, respectively. Although it was shown in ref 49 for H_2−CO that the cross sections calculated for the (j = 1, v) averaging are only slightly different from those obtained with the (j = 0, v) one, we have used the appropriate versions of $\langle r\rangle_{j,v}$ and $\langle r^2\rangle_{j,v}$ depending on the system, for the sake of the overall accuracy. The whole set of values of $\langle r\rangle_{j,v}$ and $\langle r^2\rangle_{j,v}$ are given in Table 1.

To demonstrate how the vibrational averaging affects the interaction energy surface for various isotopologues and vibrational states of H_2, we present, in Figure 1, a comparison of the interaction energy surfaces $\langle V\rangle_{j,v}(R, \theta)$, defined in eq 1,

https://dx.doi.org/10.1021/acs.jctc.0c01122
J. Chem. Theory Comput. 2021, 17, 1008−1016

Table 1. Expectation Values of $\langle r \rangle_{j,v}$ and $\langle r^2 \rangle_{j,v}$ Used in the Calculations for the $v = 0$ and 1 Vibrational States of the H_2, HD, and D_2 Molecules (in Bohr), Computed Based on the Potential Energy Values from Ref 52

	$H_2(j = 0)$	$H_2(j = 1)$	$HD(j = 0)$	$D_2(j = 0)$	$D_2(j = 1)$
$\langle r \rangle_{j,0}$	1.4487	1.4509	1.4422	1.4346	1.4356
$\langle r^2 \rangle_{j,0}$	2.1271	2.1334	2.1043	2.0777	2.0808
$\langle r \rangle_{j,1}$	1.5454	1.5476	1.5255	1.5021	1.5032
$\langle r^2 \rangle_{j,1}$	2.4741	2.4812	2.4009	2.3162	2.3196

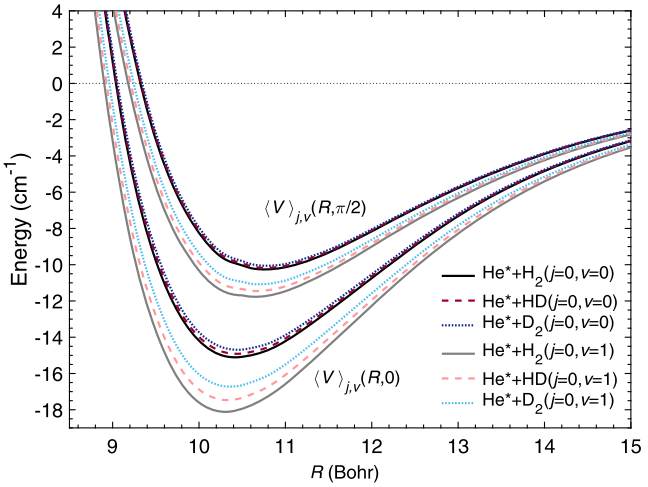

Figure 1. Interaction energy of He* + H_2/HD/D_2, where the molecule is in the ground rotational state ($j = 0$) and in the ground or first excited vibrational state ($v = 0$ or 1). Two angular orientations are chosen: the linear one ($\theta = 0$; the batch of lower curves) and the T-shaped one ($\theta = \pi/2$; the batch of upper curves).

for two angular orientations, $\theta = 0$ and $\pi/2$, as a function of the intermolecular separation R. The corresponding numerical data are provided in the Supporting Information. For $v = 0$, the curves representing different isotopologues are rather close to each other. However for $v = 1$, the differences are much larger; for example, the minimum of the interaction energy for He* + H_2 is equal to -18.1 cm^{-1}, compared to -16.7 cm^{-1} for the isotopically substituted He* + D_2. Even larger differences are due to the vibrational excitation of the molecules; for example, the minimum energy for He* + $H_2(v = 0)$ is equal to -15.1 cm^{-1}, which is 3 cm^{-1} higher than the $v = 1$ minimum, a 20% change. The position of the minimum is also shifted toward smaller values of R. Such large differences in the potentials used in the scattering calculations will be seen to result in substantial differences in the values of the rate coefficients to be discussed later.

2.2. Surface Expansion. The intermolecular potential given in eq 1 may be expanded in Legendre polynomials as follows[38]

$$\langle V \rangle_{j,v}(R, \theta) = \sum_{\eta} V_{\eta}^{(j,v)}(R) P_{\eta}(\cos \theta) \tag{2}$$

The first term, $V_0(R)$, is isotropic. The odd terms vanish for symmetric molecules, thereby the first anisotropic term for He* colliding with H_2 and D_2 is of the form $V_2(R)(3 \cos^2 \theta - 1)/2$. However, in the case of He* + HD, the center of mass of HD is not in its geometric center, and if the above expansion is carried out in the appropriate Jacobi coordinates, the V_1 term does not vanish.[55,56]

In Figure 2, we display the isotropic, V_0, and anisotropic, V_1 and V_2, radial interaction potential terms of He* + H_2/HD/D_2.

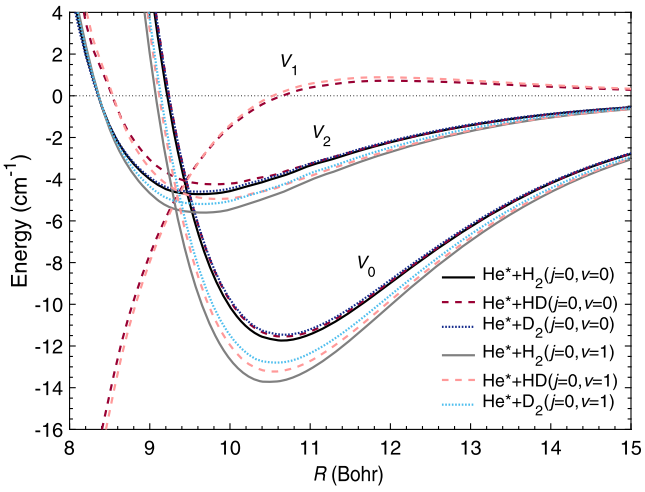

Figure 2. Isotropic (V_0) and anisotropic (V_1 and V_2) radial interaction potential terms of He* + H_2/HD/D_2, where the molecule is in the ground rotational state ($j = 0$) and in the ground or first excited vibrational state ($v = 0$ or 1).

As one could expect, the leading term V_0 is almost 3 times deeper than the corresponding V_2. The V_1 term, present for the He* + HD case, has a magnitude smaller than V_2 for $R > 9.45$ Bohr and larger for shorter intermolecular distances. This means that the repulsive wall of the V_0 potential is modified more by V_1 than by V_2. Our main interest is the dependence of the V_η terms on the masses of the molecules and their vibrational states. One can see that V_0 becomes shallower when the mass of the molecule increases. There is no such simple correlation of the depth of V_2 with the mass of the molecule. Figure 2 presents also the radial potentials when the molecule in the complex is excited to the first vibrational $v = 1$ state. The isotropic term is significantly shifted down compared to the $v = 0$ state. It should be emphasized that the anisotropy here is doubtless smaller compared to the rotational constant (B) of the colliding molecule.

2.3. Adiabatic Variational Theory (AVT) and Adiabats. The widely used method for quantum scattering calculations is close coupling. This method requires a properly prepared interaction energy surface. For instance, Balakrishnan and co-workers[57] performed close-coupling computations for cold collisions of nonexcited ^{4}He(1^1S) and ^{3}He(1^1S) with H_2 including vibrations of the molecule. However, in our studies, we have applied the recently developed adiabatic variational theory (AVT) for cold atom−diatom collision experiments.[58−60] It involves the adiabatic approximation and holds for any collision where the anisotropy of the interaction energy is small compared to the molecular rotational constant. In general, this theory allows us to reduce the multidimensional problem to a set of more easily solvable subproblems, without losing physical essence, by separating the radial from the angular motion. Thus, the interaction potential has to be expanded in terms of products of radial and angular functions, as, for example, in eq 2. Then, taking more than one nonzero term of the expansion guarantees that the anisotropy is included. AVT works well with complex potentials, where the imaginary part is related to the exponential decay rate of the entire system being in a resonance state.[61−63] In our

https://dx.doi.org/10.1021/acs.jctc.0c01122
J. Chem. Theory Comput. 2021, 17, 1008−1016

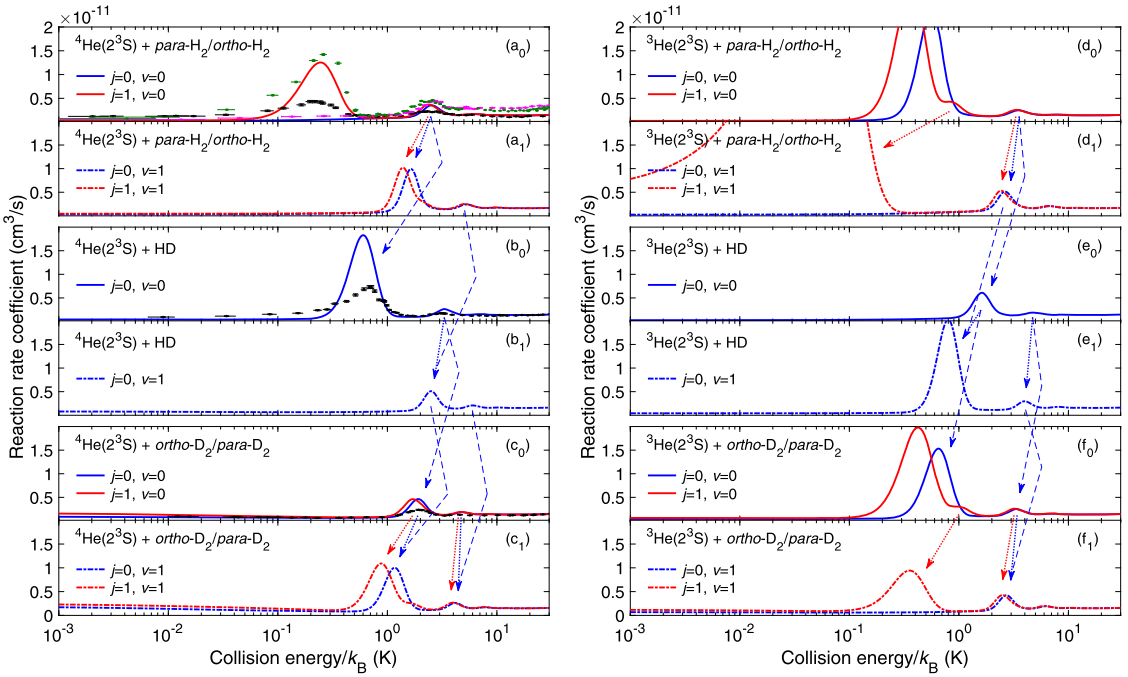

Figure 3. Theoretical and experimental reaction rate coefficients of the H_2/HD/D_2 molecules in the ground and excited rotational (j = 0/1) and vibrational (v = 0/1) states, with ^{4}He(2^3S) [left panels] or ^{3}He(2^3S) [right panels]. The theoretical results have been convoluted with the experimental energy resolution. No matching and scaling have been performed to fit the experimental data. The points with error bars are experimental values: the purple ones are for j = 0, and the green ones are for j = 1 (both taken from ref 6), whereas the black ones are for the mixture of *para* and *ortho* molecules (taken from ref 2). Note that the experimental data are burdened with systematic normalization error greater than the vertical discrepancy with respect to our results. The arrows schematically indicate the evolution of some resonances, caused by the isotopic substitution with respect to the molecule (dashed) or by the vibrational excitation of the molecule (dotted).

calculations, we have used the imaginary part from ref 62, where it was obtained by an analytical continuation to the complex plane via the Padé approximant.[64,65]

Within the framework of AVT, we construct the potential in eq 2 with the rotation terms $(\hat{l}^2/(2\mu_{A+M}R^2)$ and $B\hat{j}^2)$ in the matrix representation in the basis set of products of two spherical harmonics. Here, μ_{A+M} is the reduced mass of the complex, $\hat{l}^2$ is the operator for the end-over-end rotation of the complex, and $\hat{j}^2$ stands for the angular momentum operator of the molecule. Each matrix built for a given R (where R is a parameter) has to be diagonalized. By repeating this procedure for different values of R and ordering the eigenvalues, we obtain one-dimensional effective adiabatic potentials, known as adiabats. The technical details are described in ref 59. The adiabats asymptotically coincide with a specific rotational state of the molecule (j) as well as an end-over-end angular momentum referred to as a partial wave (l). Finally, we solve the radial Schrödinger equation separately for every adiabat. The eigensolutions serve to determine reaction rate coefficients as is shown in ref 60.

3. RESULTS AND DISCUSSION

3.1. Reaction Rate Coefficients. We have computed the PI rate coefficients for the reactions between the hydrogen isotopologues H_2, HD, and D_2, and the excited ^{4}He atoms in the metastable 2^3S state, at the wide collision temperature range, from several dozen of kelvins down to 1 mK. In a supersonic expansion, the molecular beam is cooled to the lowest rotational state with the *para*/*ortho* ratio of 1/3 for H_2 and 1/2 for D_2. Consequently, the only two states that matter are j = 0 for *para*-H_2 and *ortho*-D_2, and j = 1 for *ortho*-H_2 and *para*-D_2. Note that the HD molecule does not exhibit spin isomerism. Therefore, we first performed calculations for the vibrational ground-state hydrogen and deuterium molecules in the j = 0 and 1 rotational states, and for the rovibrational ground-state hydrogen deuteride (the j = 0 state only). These results are presented in the left panels (a_0, b_0, and c_0) of Figure 3 (see the solid blue (j = 0, v = 0) and red (j = 1, v = 0) curves). For comparison, we added all available experimental findings. Black dots with error bars represent the first-ever experimental results for H_2 (mixture *para*-H_2 and *ortho*-H_2; the a_0 panel), HD (the b_0 panel), and D_2 (mixture *ortho*-D_2 and *para*-D_2; the c_0 panel).[2] One can see that the positions of the resonances agree very well with our theoretical findings, but there is a clear difference in the relative intensities. Recently, the experiment was improved and the *para*-H_2 sample was isolated[6] from *normal*-H_2. Hence, Figure 3 also contains the reaction rate coefficients separately for ^{4}He* + *para*-H_2 and ^{4}He* + *ortho*-H_2 (purple and green dots with error bars in the top left panel, respectively). The agreement of these results with the theoretical predictions is remarkable as was discussed for this particular case in detail in our last work.[38] Unfortunately, improved PI rate coefficients for ^{4}He* + *ortho*-D_2, and indirectly for ^{4}He* + *para*-D_2, are not available.

Figure 3 clearly confirms the strong quantum kinetic isotope effect, initially discussed in ref 2. Comparing the a_0, b_0, and c_0 panels of Figure 3, one can see that the positions and intensities of the peaks are different. For instance, in the case of ^{4}He* + D_2 (the c_0 panel), there is no strong peak below 1 K. When we perform the isotopic substitution (H_2 → HD → D_2) in the theoretical calculations, there are two factors that have to be changed: the interaction energy surface and the mass of the molecule. The vibrationally averaged interaction energy becomes progressively weaker in the sequence H_2 → HD →

https://dx.doi.org/10.1021/acs.jctc.0c01122
J. Chem. Theory Comput. 2021, 17, 1008−1016

D_2 (see Figure 1), suggesting a shift of the resonances toward higher collision energies. On the other hand, the entire complex becomes heavier, which implies the opposite behavior. To see the evolution of the resonances after the isotopic substitution, let us focus on the $H_2 \rightarrow HD$ case, with the molecule in the ground rovibrational state ($j = 0$, $v = 0$). We carried out series of computations for the mass of one of the atoms in H_2 gradually changing from the mass of the hydrogen atom (m_H) to the mass of the deuterium atom (m_D), thereby nonlinearly increasing the reduced mass of the complex, and accordingly morphing the potential, $\langle V\rangle_{j=0,v=0}^{(He^* + H_2)} \rightarrow \langle V\rangle_{j=0,v=0}^{(He^* + HD)}$, as follows

$$m^{morph} = (1 - \lambda)m_H + \lambda m_D \quad (3)$$

$$V^{morph} = (1 - \lambda)\langle V\rangle_{j=0,v=0}^{(He^*+H_2)} + \lambda\langle V\rangle_{j=0,v=0}^{(He^*+HD)} \quad (4)$$

where λ is the morphing parameter that varies from 0 to 1 in steps of 0.1. The Jacobi coordinate system is adjusted to be consistent with the change of m^{morph}. Figure 4 presents the

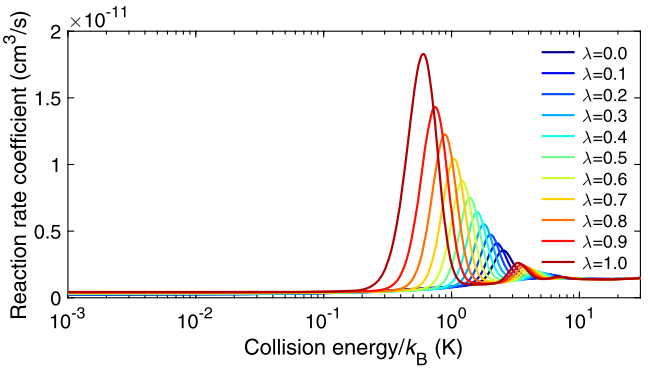

Figure 4. Reaction rate coefficients of $^4He(2^3S)$ with the rovibrational ground-state hydrogen molecule, where the mass of one of the atoms in H_2 is morphed from the H-atom mass to the D-atom one and simultaneously the interaction energy is morphed from the $^4He^* + H_2$ form to the $^4He^* + HD$ one, according to the transformation presented in eqs 3 and 4. Only the curves indicated by the values of λ equal to 0 and 1 correspond to the physical $^4He^* + para\text{-}H_2(j = 0, v = 0)$ [the a_0 panel of Figure 3] and $^4He^* + HD(j = 0, v = 0)$ [the b_0 panel of Figure 3] resonances, whereas the rest of the curves are to show the evolution from the former case into the latter one. The theoretical results have been convoluted with the experimental energy resolution.

morphed results of reaction rate coefficients, which demonstrate that the resonances move to the cold regime region when the $H_2 \rightarrow HD$ change is made. Thus, one can conclude that the effect of mass replacing in scattering calculations is stronger than the effect of changes of the potential caused by the molecule flexibility. A separate problem of the disappearance of the strongest resonances for low temperatures will be discussed in the next subsection. A similar analysis was done by one of us in ref 66 for a shape resonance in N + NH collisions. Generally, scaling the mass and the interaction energy surface is a valuable technique for understanding cold collision experiments and computations.

In our studies, we have also determined the PI rate coefficients of metastable helium colliding with the hydrogen isotopologues in the first excited vibrational state ($v = 1$). These unique results are presented as dotted-dashed curves in Figure 3. One can see that by exciting the molecule from $v = 0$ to 1, the resonant structure is dramatically changed. The low-energy resonance at 0.3 K for $^4He^* + ortho\text{-}H_2(j = 1, v = 0)$ vanishes when the *ortho*hydrogen is excited to the $v = 1$ state. A similar situation occurs for $^4He^* + HD(j = 0, v = 0 \rightarrow v = 1)$. In turn, the higher energy resonances in all cases are shifted to the lower temperature range, simultaneously increasing their intensities. A mechanism of such behavior of the resonances is explained in Section 3.2.

The right panels of Figure 3 show the reaction rate coefficients, where the $^4He^*$ atom is substituted by its stable lighter isotope, $^3He^*$. All of these results are significantly different in comparison to their counterparts from the left panels of Figure 3. Interestingly, for the $^3He^* + ortho\text{-}H_2(j = 1, v = 0)$ and $^3He^* + para\text{-}D_2(j = 1, v = 0)$ systems (compare the red curves in the d_0 and f_0 panels), the high-intensity resonances are accompanied by the much weaker ones clearly seen on their shoulders at the collision energy of $k_B \times 0.8$ K and $k_B \times 1$ K, respectively. The structure of the PI rate coefficients for the $^3He^* + ortho/para\text{-}D_2(j = 0/1, v = 1)$ collision pairs (the f_1 panel) attracted our attention, because it corresponds to the exceptional case that takes place for $^4He^* + para/ortho\text{-}H_2(j = 0/1, v = 0)$, which was widely discussed in ref 6. Let us shortly describe that issue. When the 2^3S helium atom collides with the molecular hydrogen, the extra strong resonance appears or disappears depending on the rotational state of the molecule ($j = 1$ or 0) (see the solid red and blue curves, respectively, in the top left panel of Figure 3). The origin of this low-energy resonance at 0.3 K is entirely due to the anisotropy of the interaction between $^4He^*$ and H_2.[59] When the hydrogen molecule is in the ground rotational state, its wave function is spherically symmetric and only the isotropic component of the potential is probed. Within the present work, we found $^3He^* + D_2(v = 1)$ as another example where the anisotropy in atom−molecule interactions can be directly switched on/off by the manipulation of the rotational state of the molecule, drastically affecting the PI reaction at subkelvin temperatures.

Now, we analyze the $^3He^* + ortho/para\text{-}D_2(j = 0/1)$ collisions extended in context of the vibrational state. In the f_0 and f_1 panels of Figure 3, we see two strong low-energy resonances for $v = 0$ (each for different j), whereas only one for $v = 1$. It means that by the vibrational excitation of the D_2 molecule in the lowest rotational state, the resonance vanishes. To better examine the resonances, first, we plotted in Figure 5 results without the convolution—just sharp peaks. The plot reveals that the low-energy and high-intensity convoluted resonance for $j = 1$ and $v = 0$ consists, in fact, of two closely lying resonances at about 0.5 K. The third weaker peak at 1 K corresponds, after the convolution, to the barely visible one, on the shoulder of the largest one (see the f_0 panel of Figure 3). We would like to figure out the origin of these resonances. Hence, we focus on adiabats supporting bound and resonance states in the spirit of ref 6.

3.2. Analysis Based on Adiabats. Figure 6 shows the adiabats that support the resonances discussed above and presented in Figure 5, i.e., for $^3He^* + D_2$. The adiabat in blue corresponds asymptotically to the rotational state $j = 0$, the partial wave $l = 4$, and the total angular momentum $J = 4$. The remaining three adiabats correlate asymptotically to the rotational state $j = 1$, the partial wave $l = 4$, and the total angular momenta $J = 3$, 4, 5 (yellow, red, and black curves, respectively). One can see how substantially the anisotropy

https://dx.doi.org/10.1021/acs.jctc.0c01122
J. Chem. Theory Comput. 2021, 17, 1008−1016

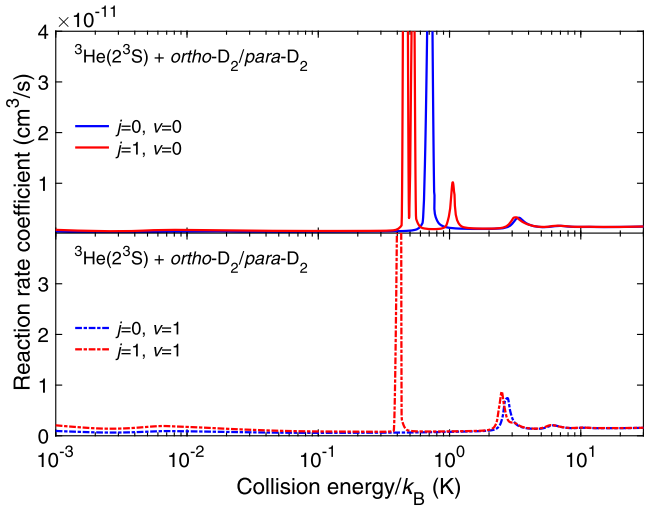

Figure 5. Theoretical reaction rate coefficients of the ^{3}He* + $D_2(j, v)$ collisions, for various values of j and v, corresponding to the data from the f_0 and f_1 panels of Figure 3, but without the convolution.

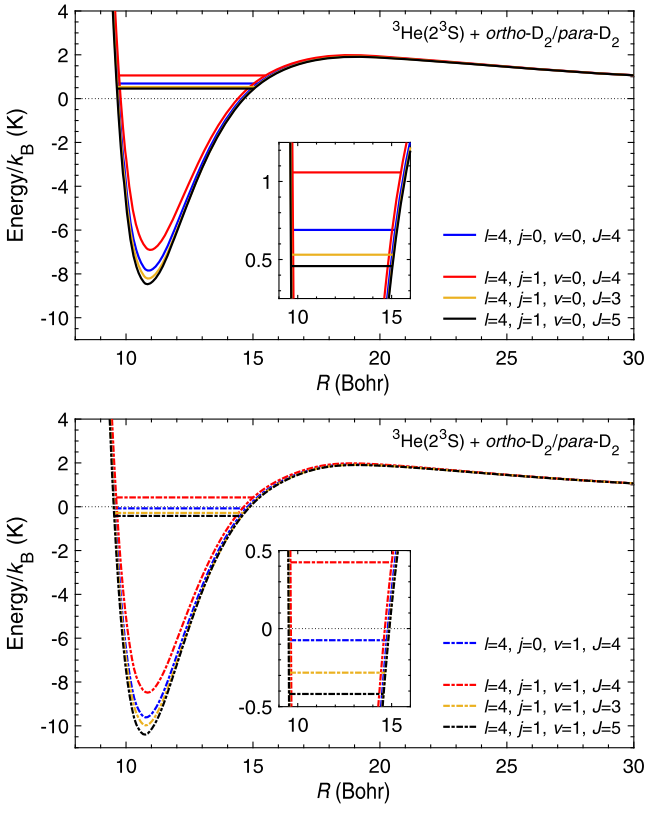

Figure 6. Effective adiabatic potentials (adiabats) as a function of intermolecular separation R for the ^{3}He(2^3S) atom colliding with *ortho*/*para*-$D_2(j = 0/1)$ in the vibrational ground ($v = 0$; top panel) and excited ($v = 1$; bottom panel) states. All adiabats here are characterized by the partial wave $l = 4$. They support the low-energy resonances. J denotes the total angular momentum, $|l - j| \leq J \leq l + j$. For pragmatic reasons, all adiabats are moved to achieve asymptotes at zero.

affects the effective potential. Each of the considered adiabats for $v = 0$ (the top panel of Figure 6) supports one resonance state whose energy level is between the dissociation threshold and the top of the barrier. When the molecule is excited to the first vibrational state ($v = 1$; the bottom panel of Figure 6), the quantum wells become deeper and then the energy levels are shifted down, three of them below the dissociation threshold. Only the state with the highest energy (in red) still remains above the threshold. In other words, three resonances turned into bound states. Consequently, the resonance observed at the collision energy of $k_B \times 0.7$ K for *ortho*-$D_2(j = 0, v = 0)$, which is shown in blue in the top panel of Figure 5, disappears in the bottom one, whereas from the three resonances placed in the range of collision energies $k_B \times (0.4, 1.1)$ K, corresponding to the *para*-$D_2(j = 1, v = 0)$ case, only one survives and is present at $k_B \times 0.4$ K in the bottom panel of Figure 5. Now, one can see that the latter resonance has the same quantum nature as the much weaker one observed as a feature on the shoulder of the strongest peak of the *para*-$D_2(j = 1, v = 0)$ case, in the f_0 panel of Figure 3.

To gain even better insight into a mechanism leading to the effects described above, we can perform the following numerical test. Let us define a surface

$$\tilde{V}^{\text{morph}} = (1 - \lambda)\langle V\rangle_{j=1,v=0} + \lambda\langle V\rangle_{j=1,v=1} \quad (5)$$

where λ is again the morphing parameter, while $\langle V\rangle_{j=1,v=0}$ and $\langle V\rangle_{j=1,v=1}$ are the surfaces averaged over the $(j = 1, v = 0)$ and $(j = 1, v = 1)$ rovibrational states of D_2, respectively. Changing the values of λ from 0 to 1, one can morph the interaction energy from the $v = 0$ form to the $v = 1$ one. Note that this time the mass of the molecule is not morphed. We have carried out calculations of the rate coefficients for the $\tilde{V}^{\text{morph}}$ potential gradually increasing λ in steps of 0.1. The results are presented

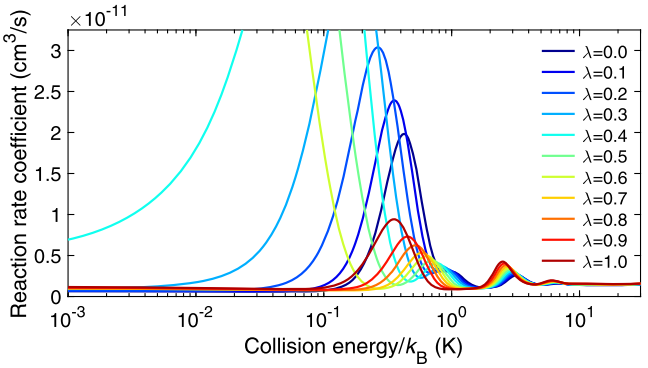

Figure 7. Reaction rate coefficients of ^{3}He(2^3S) + *para*-$D_2(j = 1)$ with the interaction energy morphed from the $v = 0$ vibrational form to the $v = 1$ one, according to the following transformation: $\tilde{V}^{\text{morph}} = (1 - \lambda)\langle V\rangle_{j=1,v=0} + \lambda\langle V\rangle_{j=1,v=1}$, where $\lambda \in [0, 1]$, see eq 5. The theoretical results have been convoluted with the experimental energy resolution.

in Figure 7, and we can see that the convoluted resonance for ^{3}He* + *para*-$D_2(j = 1, v = 0)$ at 1 K becomes the resonance at 0.4 K for $v = 1$, whereas the convoluted low-energy resonance at 0.5 K, which in fact consists of two closely lying resonances, shifts toward lower temperatures, and finally vanishes. A similar analysis (with adiabats and morphing) can be done for every $v = 0$ and 1 pair of panels presented in Figure 3 as well as for every pair of the $j = 0$ and 1 states considered in this work, since the mechanism of appearance and disappearance of resonances is the same. Moreover, it can be also performed for the isotopic substitution.

https://dx.doi.org/10.1021/acs.jctc.0c01122
J. Chem. Theory Comput. 2021, 17, 1008−1016

4. CONCLUSIONS

This paper shows the very accurate theoretical results of PI rate coefficients for all possible combinations of ^{4}He and ^{3}He in the metastable 2^3S state colliding with the hydrogen isotopologues (H_2, HD, D_2) in the two lowest rotational and vibrational states at subkelvin temperatures. For all but the ^{4}He* + *para*/*ortho*-$H_2(v = 0)$ cases, these are the first theoretical results of such high quality. The calculations have been carried out based on the best available *ab initio* interaction energy surface, developed by us,[38] which includes molecule nonrigidity effects. The results confirm the recently observed strong quantum kinetic isotope effect in cold collisions.[2] The rate of the PI process can differ by as much as an order of magnitude at certain collision energies depending on the isotope or isotopologue. We have demonstrated that the existence of resonances is determined by the position of energy levels in quantum wells formed by adiabats. Consequently, the location of major peaks in the reaction rate coefficients can be controlled by the rovibrational state of the molecule. In sum, the change of the rotational and vibrational quantum numbers of the molecule can strongly enhance or suppress the PI reaction like a quantum switch. Moreover, we have presented the origin of the resonances and the mechanism of their disappearance. This was supported by model calculations with the morphed mass and interaction potential. We are positive that our findings are an important contribution to a precise control of chemical reactions in cold chemistry. Since nowadays the vibrational excitation of the hydrogen isotopologues is feasible,[39−41] our work calls for new experiments in this field.

■ ASSOCIATED CONTENT

Supporting Information

The Supporting Information is available free of charge at https://pubs.acs.org/doi/10.1021/acs.jctc.0c01122.

Values of the interaction potential of He* + H_2/HD/D_2 for two angular orientations: the linear one ($\theta = 0$) and the T-shaped one ($\theta = \pi/2$) (PDF)

■ AUTHOR INFORMATION

Corresponding Author

Mariusz Pawlak − *Faculty of Chemistry, Nicolaus Copernicus University in Toruń, 87-100 Toruń, Poland;* orcid.org/0000-0002-2200-8287; Email: teomar@chem.umk.pl

Authors

Piotr S. Żuchowski − *Faculty of Physics, Astronomy and Informatics, Nicolaus Copernicus University in Toruń, 87-100 Toruń, Poland;* orcid.org/0000-0001-9267-3090

Piotr Jankowski − *Faculty of Chemistry, Nicolaus Copernicus University in Toruń, 87-100 Toruń, Poland*

Complete contact information is available at: https://pubs.acs.org/10.1021/acs.jctc.0c01122

Notes

The authors declare no competing financial interest.

■ ACKNOWLEDGMENTS

This research was financially supported by the National Science Centre, Poland (grant no. 2016/23/D/ST4/00341 [M.P.], grant no. 2015/19/B/ST4/02707 [P.S.Ż.], and grant no. 2017/25/B/ST4/01300 [P.J.]).

■ REFERENCES

(1) Henson, A. B.; Gersten, S.; Shagam, Y.; Narevicius, J.; Narevicius, E. Observation of Resonances in Penning Ionization Reactions at Sub-Kelvin Temperatures in Merged Beams. *Science* **2012**, *338*, 234−238.

(2) Lavert-Ofir, E.; Shagam, Y.; Henson, A. B.; Gersten, S.; Kłos, J.; Żuchowski, P. S.; Narevicius, J.; Narevicius, E. Observation of the isotope effect in sub-kelvin reactions. *Nat. Chem.* **2014**, *6*, 332−335.

(3) Jankunas, J.; Bertsche, B.; Jachymski, K.; Hapka, M.; Osterwalder, A. Dynamics of gas phase Ne* + NH_3 and Ne* + ND_3 Penning ionisation at low temperatures. *J. Chem. Phys.* **2014**, *140*, No. 244302.

(4) Jankunas, J.; Bertsche, B.; Osterwalder, A. Study of the Ne($^3P_2$) + CH_3F Electron-Transfer Reaction below 1 K. *J. Phys. Chem. A* **2014**, *118*, 3875−3879.

(5) Shagam, Y.; Klein, A.; Skomorowski, W.; Yun, R.; Averbukh, V.; Koch, C. P.; Narevicius, E. Molecular hydrogen interacts more strongly when rotationally excited at low temperatures leading to faster reactions. *Nat. Chem.* **2015**, *7*, 921−926.

(6) Klein, A.; Shagam, Y.; Skomorowski, W.; Żuchowski, P. S.; Pawlak, M.; Moiseyev, N.; Janssen, M. C.; van de Meerakker, S. Y. T.; van der Avoird, A.; Koch, C. P.; Narevicius, E. Directly probing anisotropy in atom-molecule collisions through quantum scattering resonances. *Nat. Phys.* **2017**, *13*, 35−38.

(7) Gordon, S. D. S.; Omiste, J. J.; Zou, J.; Tanteri, S.; Brumer, P.; Osterwalder, A. Quantum-state-controlled channel branching in cold Ne($^3P_2$)+Ar chemi-ionization. *Nat. Chem.* **2018**, *10*, 1190−1195.

(8) Zou, J.; Gordon, S. D. S.; Osterwalder, A. Sub-Kelvin Stereodynamics of the Ne($^3P_2$)+N_2 Reaction. *Phys. Rev. Lett.* **2019**, *123*, No. 133401.

(9) Blech, A.; Shagam, Y.; Hölsch, N.; Paliwal, P.; Skomorowski, W.; Rosenberg, J. W.; Bibelnik, N.; Heber, O.; Reich, D. M.; Narevicius, E.; Koch, C. P. Phase protection of Fano-Feshbach resonances. *Nat. Commun.* **2020**, *11*, No. 999.

(10) Margulis, B.; Narevicius, J.; Narevicius, E. Direct observation of a Feshbach resonance by coincidence detection of ions and electrons in Penning ionization collisions. *Nat. Commun.* **2020**, *11*, No. 3553.

(11) Jankunas, J.; Osterwalder, A. Cold and Controlled Molecular Beams: Production and Applications. *Annu. Rev. Phys. Chem.* **2015**, *66*, 241−262.

(12) Balakrishnan, N. Perspective: Ultracold molecules and the dawn of cold controlled chemistry. *J. Chem. Phys.* **2016**, *145*, No. 150901.

(13) Bohn, J. L.; Rey, A. M.; Ye, J. Cold molecules: Progress in quantum engineering of chemistry and quantum matter. *Science* **2017**, *357*, 1002−1010.

(14) *Cold Chemistry*; Dulieu, O.; Osterwalder, A., Eds.; Theoretical and Computational Chemistry Series; The Royal Society of Chemistry, 2018; pp P001−P670.

(15) Koch, C. P.; Lemeshko, M.; Sugny, D. Quantum control of molecular rotation. *Rev. Mod. Phys.* **2019**, *91*, No. 035005.

(16) Messenger, S. Identification of molecular-cloud material in interplanetary dust particles. *Nature* **2000**, *404*, 968−971.

(17) Millar, T. J. Deuterium Fractionation in Interstellar Clouds. *Space Sci. Rev.* **2003**, *106*, 73−86.

(18) Dalgarno, A. *Molecular Hydrogen in Space*; Combes, F.; Pineau des Forêts, G., Eds.; Cambridge Contemporary Astrophysics; Cambridge University Press, 2000; pp 3−12.

(19) Spake, J. J.; Sing, D. K.; Evans, T. M.; Oklopčić, A.; Bourrier, V.; Kreidberg, L.; Rackham, B. V.; Irwin, J.; Ehrenreich, D.; Wyttenbach, A.; Wakeford, H. R.; Zhou, Y.; Chubb, K. L.; Nikolov, N.; Goyal, J. M.; Henry, G. W.; Williamson, M. H.; Blumenthal, S.; Anderson, D. R.; Hellier, C.; Charbonneau, D.; Udry, S.; Madhusudhan, N. Helium in the eroding atmosphere of an exoplanet. *Nature* **2018**, *557*, 68−70.

(20) Hubbard, W. B. Neptune's Deep Chemistry. *Science* **1997**, *275*, 1279−1280.

(21) Allart, R.; Bourrier, V.; Lovis, C.; Ehrenreich, D.; Spake, J. J.; Wyttenbach, A.; Pino, L.; Pepe, F.; Sing, D. K.; Lecavelier des Etangs,

A. Spectrally resolved helium absorption from the extended atmosphere of a warm Neptune-mass exoplanet. *Science* **2018**, *362*, 1384−1387.
(22) Nortmann, L.; Pallé, E.; Salz, M.; Sanz-Forcada, J.; Nagel, E.; Alonso-Floriano, F. J.; Czesla, S.; Yan, F.; Chen, G.; Snellen, I. A. G.; Zechmeister, M.; Schmitt, J. H. M. M.; López-Puertas, M.; Casasayas-Barris, N.; Bauer, F. F.; Amado, P. J.; Caballero, J. A.; Dreizler, S.; Henning, T.; Lampón, M.; Montes, D.; Molaverdikhani, K.; Quirrenbach, A.; Reiners, A.; Ribas, I.; Sánchez-López, A.; Schneider, P. C.; Zapatero Osorio, M. R. Ground-based detection of an extended helium atmosphere in the Saturn-mass exoplanet WASP-69b. *Science* **2018**, *362*, 1388−1391.
(23) Salz, M.; Czesla, S.; Schneider, P. C.; Nagel, E.; Schmitt, J. H. M. M.; Nortmann, L.; Alonso-Floriano, F. J.; López-Puertas, M.; Lampón, M.; Bauer, F. F.; Snellen, I. A. G.; Pallé, E.; Caballero, J. A.; Yan, F.; Chen, G.; Sanz-Forcada, J.; Amado, P. J.; Quirrenbach, A.; Ribas, I.; Reiners, A.; Béjar, V. J. S.; Casasayas-Barris, N.; Cortés-Contreras, M.; Dreizler, S.; Guenther, E. W.; Henning, T.; Jeffers, S. V.; Kaminski, A.; Kürster, M.; Lafarga, M.; Lara, L. M.; Molaverdikhani, K.; Montes, D.; Morales, J. C.; Sánchez-López, A.; Seifert, W.; Zapatero Osorio, M. R.; Zechmeister, M. Detection of He I λ10830 Å absorption on HD 189733 b with CARMENES high-resolution transmission spectroscopy. *Astron. Astrophys.* **2018**, *620*, A97.
(24) Mansfield, M.; Bean, J. L.; Oklopčić, A.; Kreidberg, L.; Désert, J.-M.; Kempton, E. M.-R.; Line, M. R.; Fortney, J. J.; Henry, G. W.; Mallonn, M.; Stevenson, K. B.; Dragomir, D.; Allart, R.; Bourrier, V. Detection of Helium in the Atmosphere of the Exo-Neptune HAT-P-11b. *Astrophys. J. Lett.* **2018**, *868*, L34.
(25) Allart, R.; Bourrier, V.; Lovis, C.; Ehrenreich, D.; Aceituno, J.; Guijarro, A.; Pepe, F.; Sing, D. K.; Spake, J. J.; Wyttenbach, A. High-resolution confirmation of an extended helium atmosphere around WASP-107b. *Astron. Astrophys.* **2019**, *623*, A58.
(26) Alonso-Floriano, F. J.; Snellen, I. A. G.; Czesla, S.; Bauer, F. F.; Salz, M.; Lampón, M.; Lara, L. M.; Nagel, E.; López-Puertas, M.; Nortmann, L.; Sánchez-López, A.; Sanz-Forcada, J.; Caballero, J. A.; Reiners, A.; Ribas, I.; Quirrenbach, A.; Amado, P. J.; Aceituno, J.; Anglada-Escudé, G.; Béjar, V. J. S.; Brinkmöller, M.; Hatzes, A. P.; Henning, T.; Kaminski, A.; Kürster, M.; Labarga, F.; Montes, D.; Pallé, E.; Schmitt, J. H. M. M.; Zapatero Osorio, M. R. He I λ 10830 Å in the transmission spectrum of HD 209458 b. *Astron. Astrophys.* **2019**, *629*, A110.
(27) Kirk, J.; Alam, M. K.; López-Morales, M.; Zeng, L. Confirmation of WASP-107b's Extended Helium Atmosphere with Keck II/NIRSPEC. *Astron. J.* **2020**, *129*, 115.
(28) Ninan, J. P.; Stefansson, G.; Mahadevan, S.; Bender, C.; Robertson, P.; Ramsey, L.; Terrien, R.; Wright, J.; Diddams, S. A.; Kanodia, S.; Cochran, W.; Endl, M.; Ford, E. B.; Fredrick, C.; Halverson, S.; Hearty, F.; Jennings, J.; Kaplan, K.; Lubar, E.; Metcalf, A. J.; Monson, A.; Nitroy, C.; Roy, A.; Schwab, C. Evidence for He I 10830 Å Absorption during the Transit of a Warm Neptune around the M-dwarf GJ 3470 with the Habitable-zone Planet Finder. *Astron. J.* **2020**, *894*, 97.
(29) Vissapragada, S.; Knutson, H. A.; Jovanovic, N.; Harada, C. K.; Oklopčić, A.; Eriksen, J.; Mawet, D.; Millar-Blanchaer, M. A.; Tinyanont, S.; Vasisht, G. Constraints on Metastable Helium in the Atmospheres of WASP-69b and WASP-52b with Ultranarrowband Photometry. *Astron. J.* **2020**, *159*, 278.
(30) Falcinelli, S.; Candori, P.; Bettoni, M.; Pirani, F.; Vecchiocattivi, F. Penning Ionization Electron Spectroscopy of Hydrogen Sulfide by Metastable Helium and Neon Atoms. *J. Phys. Chem. A* **2014**, *118*, 6501−6506.
(31) Biondini, F.; Brunetti, B. G.; Candori, P.; De Angelis, F.; Falcinelli, S.; Tarantelli, F.; Moix Teixidor, M.; Pirani, F.; Vecchiocattivi, F. Penning ionization of N_2O molecules by He*($2^{3,1}$S) and Ne*($^3P_{2,0}$) metastable atoms: A crossed beam study. *J. Chem. Phys.* **2005**, *122*, No. 164307.
(32) Yamazaki, M.; Maeda, S.; Kishimoto, N.; Ohno, K. Penning ionization electron spectroscopy of C_6H_6 by collision with He*(2^3S) metastable atoms and classical trajectory calculations: Optimization of ab initio model potentials. *J. Chem. Phys.* **2005**, *122*, No. 044303.
(33) Yamauchi, M.; Yamakita, Y.; Yamakado, H.; Ohno, K. Collision energy resolved Penning ionization electron spectra of polycyclic aromatic hydrocarbons. *J. Electron Spectrosc. Relat. Phenom.* **1998**, *88*−*91*, 155−161.
(34) Yamakita, Y.; Yamauchi, M.; Ohno, K. Penning ionization of [2,2]-paracyclophane by collision with metastable He*(2^3S) atoms. *Chem. Phys. Lett.* **2000**, *322*, 189−198.
(35) Yamakita, Y.; Yamauchi, M.; Ohno, K. Penning ionization electron spectra of pyrene, chrysene, and coronene in collision with metastable He(2^3S) atoms in the gas phase. *J. Chem. Phys.* **2009**, *130*, No. 024306.
(36) Yamakita, Y.; Ohno, K. Collision-Energy-Resolved Penning Ionization Electron Spectroscopy of Glycine with He(2^3S) Metastable Atoms: Conformational Isomers in Collisional Ionization. *J. Phys. Chem. A* **2009**, *113*, 10779−10786.
(37) Ishiguro, Y.; Yamakita, Y.; Hayashi, N. Penning ionization electron spectroscopy of anisole, thioanisole, and selenoanisole by collision with He*(2^3S): Conjugation effects and conformational stability. *Chem. Phys. Lett.* **2020**, *754*, No. 137653.
(38) Pawlak, M.; Żuchowski, P. S.; Moiseyev, N.; Jankowski, P. Evidence of Nonrigidity Effects in the Description of Low-Energy Anisotropic Molecular Collisions of Hydrogen Molecules with Excited Metastable Helium Atoms. *J. Chem. Theory Comput.* **2020**, *16*, 2450−2459.
(39) Wang, T.; Yang, T.; Xiao, C.; Dai, D.; Yang, X. Highly Efficient Pumping of Vibrationally Excited HD Molecules via Stark-Induced Adiabatic Raman Passage. *J. Phys. Chem. Lett.* **2013**, *4*, 368−371.
(40) Dong, W.; Mukherjee, N.; Zare, R. N. Optical preparation of H_2 rovibrational levels with almost complete population transfer. *J. Chem. Phys.* **2013**, *139*, No. 074204.
(41) Wang, T.; Chen, J.; Yang, T.; Xiao, C.; Sun, Z.; Huang, L.; Dai, D.; Yang, X.; Zhang, D. H. Dynamical Resonances Accessible Only by Reagent Vibrational Excitation in the F+HD→HF+D Reaction. *Science* **2013**, *342*, 1499−1502.
(42) Jeziorska, M.; Jankowski, P.; Szalewicz, K.; Jeziorski, B. On the optimal choice of monomer geometry in calculations of intermolecular interaction energies: Rovibrational spectrum of Ar-HF from two- and three-dimensional potentials. *J. Chem. Phys.* **2000**, *113*, 2957−2968.
(43) Jankowski, P. Approximate generation of full-dimensional ab initio van der Waals surfaces for high-resolution spectroscopy. *J. Chem. Phys.* **2004**, *121*, 1655−1662.
(44) Jankowski, P.; Szalewicz, K. A new ab initio interaction energy surface and high-resolution spectra of the H_2-CO van der Waals complex. *J. Chem. Phys.* **2005**, *123*, No. 104301.
(45) Jankowski, P.; McKellar, A. R. W.; Szalewicz, K. Theory Untangles the High-Resolution Infrared Spectrum of the ortho-H_2-CO van der Waals Complex. *Science* **2012**, *336*, 1147−1150.
(46) Jankowski, P.; Surin, L. A.; Potapov, A. V.; Schlemmer, S.; McKellar, A. R. W.; Szalewicz, K. A comprehensive experimental and theoretical study of H_2-CO spectra. *J. Chem. Phys.* **2013**, *138*, No. 084307.
(47) Jankowski, P. Exploring the new three-dimensional ab initio interaction energy surface of the Ar-HF complex: Rovibrational calculations for Ar-HF and Ar-DF with vibrationally excited diatoms. *J. Chem. Phys.* **2008**, *128*, No. 154311.
(48) Jankowski, P.; Szalewicz, K. Effects of monomer flexibility on spectra of N_2-HF. *Chem. Phys. Lett.* **2008**, *459*, 60−64.
(49) Faure, A.; Jankowski, P.; Stoecklin, T.; Szalewicz, K. On the importance of full-dimensionality in low-energy molecular scattering calculations. *Sci. Rep.* **2016**, *6*, No. 28449.
(50) Chefdeville, S.; Stoecklin, T.; Naulin, C.; Jankowski, P.; Szalewicz, K.; Faure, A.; Costes, M.; Bergeat, A. Experimental and theoretical analysis of low-energy CO + H_2 inelastic collisions. *Astrophys. J., Lett.* **2015**, *799*, 1−4.
(51) Stoecklin, T.; Faure, A.; Jankowski, P.; Chefdeville, S.; Bergeat, A.; Naulin, C.; Morales, S.; Costes, M. Comparative experimental and

https://dx.doi.org/10.1021/acs.jctc.0c01122
J. Chem. Theory Comput. 2021, 17, 1008−1016

theoretical study of the rotational excitation of CO by collisions with ortho- and para-D_2 molecules. *Phys. Chem. Chem. Phys.* **2017**, *19*, 189−195.
(52) Kołos, W.; Szalewicz, K.; Monkhorst, H. J. New Born−Oppenheimer potential energy curve and vibrational energies for the electronic ground state of the hydrogen molecule. *J. Chem. Phys.* **1986**, *84*, 3278−3283.
(53) Jeziorski, B.; Moszynski, R.; Szalewicz, K. Perturbation Theory Approach to Intermolecular Potential Energy Surfaces of van der Waals Complexes. *Chem. Rev.* **1994**, *94*, 1887−1930.
(54) Handy, N. C.; Yamaguchi, Y.; Schaefer, H. F., III The diagonal correction to the Born-Oppenheimer approximation: Its effect on the singlet-triplet splitting of CH_2 and other molecular effects. *J. Chem. Phys.* **1986**, *84*, 4481−4484.
(55) Kreek, H.; Le Roy, R. J. Intermolecular potentials and isotope effects for molecular hydrogen-inert gas complexes. *J. Chem. Phys.* **1975**, *63*, 338−344.
(56) Liu, W. K.; Grabenstetter, J. E.; Le Roy, R. J.; McCourt, F. R. Effect of asymmetric isotopic substitution on atom-diatom potentials. *J. Chem. Phys.* **1978**, *68*, 5028−5031.
(57) Balakrishnan, N.; Forrey, R. C.; Dalgarno, A. Quenching of H_2 Vibrations in Ultracold ^{3}He and ^{4}He Collisions. *Phys. Rev. Lett.* **1998**, *80*, 3224−3227.
(58) Pawlak, M.; Shagam, Y.; Narevicius, E.; Moiseyev, N. Adiabatic theory for anisotropic cold molecule collisions. *J. Chem. Phys.* **2015**, *143*, No. 074114.
(59) Pawlak, M.; Shagam, Y.; Klein, A.; Narevicius, E.; Moiseyev, N. Adiabatic Variational Theory for Cold Atom-Molecule Collisions: Application to a Metastable Helium Atom Colliding with ortho- and para-Hydrogen Molecules. *J. Phys. Chem. A* **2017**, *121*, 2194−2198.
(60) Pawlak, M.; Ben-Asher, A.; Moiseyev, N. Simple Closed-Form Expression for Penning Reaction Rate Coefficients for Cold Molecular Collisions by Non-Hermitian Time-Independent Adiabatic Scattering Theory. *J. Chem. Theory Comput.* **2018**, *14*, 236−241.
(61) Moiseyev, N. *Non-Hermitian Quantum Mechanics*; Cambridge University Press: Cambridge, 2011.
(62) Bhattacharya, D.; Ben-Asher, A.; Haritan, I.; Pawlak, M.; Landau, A.; Moiseyev, N. Polyatomic ab initio Complex Potential Energy Surfaces: Illustration of Ultracold Collisions. *J. Chem. Theory Comput.* **2017**, *13*, 1682−1690.
(63) Bhattacharya, D.; Pawlak, M.; Ben-Asher, A.; Landau, A.; Haritan, I.; Narevicius, E.; Moiseyev, N. Quantum Effects in Cold Molecular Collisions from Spatial Polarization of Electronic Wave Function. *J. Phys. Chem. Lett.* **2019**, *10*, 855−863.
(64) Landau, A.; Haritan, I.; Kaprálová-Zďánská, P. R.; Moiseyev, N. Atomic and Molecular Complex Resonances from Real Eigenvalues Using Standard (Hermitian) Electronic Structure Calculations. *J. Phys. Chem. A* **2016**, *120*, 3098−3108.
(65) Landau, A.; Bhattacharya, D.; Haritan, I.; Ben-Asher, A.; Moiseyev, N. Ab initio Complex Potential Energy Surfaces from Standard Quantum Chemistry Packages. *Adv. Quantum Chem.* **2017**, *74*, 321−346.
(66) Żuchowski, P. S.; Hutson, J. M. Cold collisions of N (^4S) atoms and NH ($^3\sum$) molecules in magnetic fields. *Phys. Chem. Chem. Phys.* **2011**, *13*, 3669−3680.

https://dx.doi.org/10.1021/acs.jctc.0c01122
J. Chem. Theory Comput. 2021, 17, 1008−1016